Code Design For Automotive MIMO Radar

Oded Bialer [1], Amnon Jonas [1], and Tom Tirer [1,2]
[1]General Motors - Advanced Technical Center Israel
[2]School of Electrical Engineering, Tel Aviv University, Israel

***Abstract*—Fast chirp FMCW modulation with code division multiple access (CDMA) for multiple input multiple output (MIMO) radar is a commonly used technique for automotive radar, since it efficiently provides high range and angel resolution, as well as a long detection range. However, the ambiguity function of the fast chirp FMCW CDMA MIMO radar has high side-lobes in the Doppler domain, which degrade the detection performance in the case of multiple targets at similar range. In this paper, we consider the case of multiple targets that overlap in range, but during a detection interval their range difference migrates proportionally to the Doppler frequency difference between them. We derive an analytical expression for the ambiguity function in this case. From the analytical expression we obtain insight that high detection performance is achieved when the code attenuates the ambiguity function side-lobes inversely proportional to the Doppler frequency difference from the main-lobe. Therefore, we design a code sequence and FMCW chirp transmission times that jointly achieve this objective, and show the performance advantage in the probability of detection of the proposed approach compared to other reference methods.**

I. Introduction

Automotive radar is a key sensor for autonomous driving due to its long detection range [1]. Multiple input multiple output (MIMO) radar is an efficient method for obtaining high angular resolution with a relatively small number of antennas [2]. MIMO radar requires separating between multiple antenna transmissions at the receive antennas, which can be achieved with code division multiple access (CDMA). In CDMA, all the antennas transmit simultaneously separate coding sequences that enable to separate them at the receiver [3].

Fast chirp FMCW is widely used transmission waveform for automotive radar [4] since it enables to transmit a wide RF bandwidth that provides high range resolution, with small base-band bandwidth. The common approach in automotive radar for combining CDMA with fast chirp FMCW is inter-chirp coding, where each chirp is multiplied with a separate code symbol [5]. Inter-chirp coding provides significantly lower side-lobes in the ambiguity function along the range domain compared intra-chirp coding [6], which is essentially in the automotive scenario because there is often a large difference in the received power between close and far objects.

The advantage of CDMA is that it has high emission power due to simultaneous transmissions without redundancy in frequency bandwidth. Its disadvantage is high side-lobes in the radar's ambiguity function, in particular in the Doppler domain. The ambiguity function of the radar is the match filter output for a point target over hypotheses of range, Doppler and angle [7]. The automotive radar scenarios typically include many objects, and hence the match filter output is a superposition of the ambiguity functions from all the reflection points. Therefore, high side-lobes in the ambiguity function degrade the detection performance of the radar.

In CDMA MIMO the ambiguity function main-lobe to side-lobe ratio depends on the CDMA code. Gold codes and other codes [6]-[9] obtain low correlation between code sequences with a delay shift, but do not have low correlation between code sequences when there is a Doppler frequency shift. Hence these codes are good codes for direct-sequence spread spectrum pulse-modulated continuous wave (PMCW) radar [10] but are less suited for fast chirp FMCW radars with inter-chirp coding.

Chen and Vaidyanathan [11] have formulated the signal to interference ratio (SINR) as a function of the extended target and clutter statistics, and optimized the MIMO radar code to minimize the SINR. This approach is less applicable for the automotive radar since there are many different targets and clutter scenarios, thus they are difficult to model.

Repetitions of a short Hadamard code sequence or DDMA coding result in grating lobes in the Doppler domain of the ambiguity function that cause severe Doppler ambiguity issues [3],[12]. On the other hand, long orthogonal codes, dithered DDMA codes, and also long pseudo random codes, such as maximum length sequences (M-sequences) [13]-[15], eliminate the grating lobes, and have a relatively flat side-lobes across the Doppler spectrum, with a peak to side-lobe ratio that is equal to the code sequence length.

Prior MIMO radar code design methods have considered the ambiguity function over a short coherent frame duration, in which targets ranges are fixed, and hence masking between targets at the same range is eternally. However, in automotive applications, the duration for target detection, referred to as detection interval, is longer than the coherent processing interval, and typically includes detection from a series of frames. During the detection interval the difference between the targets ranges migrates proportionally to the Doppler difference between them. Targets with large Doppler difference will overlap in range for only a short time during the detection interval. Hence targets with large Doppler difference interfere each other less then targets with small Doppler difference.

In this paper, we derive an analytical expression for the ambiguity function taking into account the range migration during the detection interval. We show that the side-lobes of this ambiguity function are minimized when the code and chirps timing are designed to attenuates the side-lobes at Doppler frequencies that are near the main-lobe, at the expense of increasing the side-lobes at frequencies that are far from the main-lobe. The reason is that targets with small Doppler difference have a small velocity difference, and

ISBN: 978-9-0827-9706-0

hence when they are at close range they will be masking each other for a longer duration than targets that have large Doppler differences. We introduce a code and chirp timing design method that achieves this objective and demonstrate its detection performance advantage compared to reference methods in the case of multiple targets.

II. System model and problem formulation

The radar system considered in this paper has N_{Tx} transmit antennas, and each antenna transmits M chirps, where each chirp is multiplied with a code symbol. The transmitted signal from the l^{th} transmit antenna can be expressed by

$$x_l(t) = \sum_{m=0}^{M-1} c_m^l u(t - T_m), \tag{1}$$

where $u(t)$ is a chirp signal given by

$$u(t) = \left\{ \begin{array}{cc} sin(2\pi f_c t + 2\pi\alpha t^2) & 0 \leq t \leq T_u \\ 0 & otherwise \end{array} \right\}, \tag{2}$$

f_c is the carrier frequency, α is the chirp slope, T_u is the chirp duration, T_m is the transmission time of the m^{th} chirp, and c_i^l is the i^{th} code symbol from the l^{th} transmitter. The code symbols from all the transmit antennas are represented by a code matrix with dimension $N_{Tx} \times M$, which is given by

$$\boldsymbol{C} = \left[\begin{array}{cccc} c_0^0 & c_1^0 & .. & c_{M-1}^0 \\ \vdots & \vdots & \cdots & \vdots \\ c_0^{N_{Tx}-1} & c_1^{N_{Tx}-1} & .. & c_{M-1}^{N_{Tx}-1} \end{array} \right]. \tag{3}$$

The reflected signal is received at N_{Rx} radar antennas, and then standard FMCW MIMO radar match filter processing is applied [2], as follows. The received signal from each antenna is multiplied with a reference transmitted chirp signal, resulting in a down-converted chirp signal. Then, range stretch processing is applied by discrete Fourier transform (DFT) per chirp, followed by dot product with the code sequence of each transmitter, Doppler DFT along chirps, and beamforming. Finally, detection points are obtained by a constant false alarm rate (CFAR) algorithm [16] operating on the beamforming output.

Let T_D be the maximal allowed time interval for detecting a target, referred to as the detection interval. In this paper, we consider the worst case in terms of the probability of detection, which is illustrated in Fig. 1. In this case, multiple targets overlap in range at the middle of the detection interval. The ranges of the targets migrate during the detection interval proportionally to their Doppler frequency. In the worst case conditions the maximal range difference between the target is at the detection interval edges (after duration of $T_D/2$ from when the targets overlap), and is given by

$$r_0 - r = \frac{\epsilon}{2f_c}(f_0 - f)\frac{T_D}{2} = \frac{\lambda T_D(f_0 - f)}{4}, \tag{4}$$

where ϵ denotes the speed of light, λ is the wavelength, and $r_0 - r$, $f_0 - f$ are the range and Doppler differences between targets, respectively. This is the worst case, since any other time in which the targets ranges overlap during the detection interval, would result in larger range difference than (4) in one of the detection interval edges then.

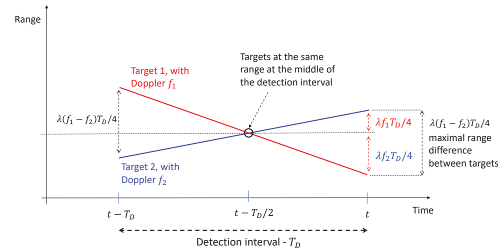

Fig. 1: Worst case in terms of the detection interval.

The best detection conditions in the worst case scenario are at the interval edges of Fig. 1, because there the range difference between the targets is maximal. Therefore, we approximate the detection performance over the entire interval in Fig. 1 by the performance at the edges of the interval, where the range difference between the targets is given in (4). The problem at hand is finding a code, $\boldsymbol{C}$, and fast chirp FMCW transmission times, $T_0, T_1, .., T_{M-1}$, that achieve high probability of detection with low probability of false alarm, when the range difference between the targets is given by (4).

III. Code and Chips Timing Design

In the case of multiple targets the detection performance of a radar improves as the peak to side-lobe ratio of its ambiguity function increases [7]. The radar's ambiguity function is the match filter output for single point target [7], i.e., the beamforming output in the case of a single point reflector. For a point target at Doppler, angle, and range f_0, θ_0, r_0, respectively, the ambiguity function value at the Doppler, angle and range hypotheses, f, θ, r, respectively, can be expressed by

$$\tilde{J}(\theta, f, r, \theta_0, f_0, r_0) = \left|\gamma(\theta, f, \theta_0, f_0)\right|^2 \left|s(r_0 - r)\right|^2, \tag{5}$$

where

$$s(r_0 - r) = \sum_{n=0}^{L-1} e^{j2\pi\alpha(r0-r)T_s/\epsilon}, \tag{6}$$

is the range processing DFT output at range hypothesis r,

$$\gamma(\theta, f, \theta_0, f_0) = \text{vec}\left(\boldsymbol{Y}(\theta, f)\right)^H \text{vec}\left(\boldsymbol{Y}(\theta_0, f_0)\right), \tag{7}$$

is the Doppler DFT and beamforming output at f, θ respectively, where $\text{vec}(\cdot)$ is column-wise vectorization,

$$\boldsymbol{Y}(\theta, f) = \boldsymbol{a}_{Rx}(\theta)\boldsymbol{a}_{Tx}^T(\theta)\boldsymbol{C}\boldsymbol{D}(f), \tag{8}$$

is the received coded symbols at the N_{Rx} antennas,

$$\boldsymbol{D}(f) = \text{diag}\{1, e^{j2\pi f T_0}, e^{j2\pi f 2T_1}, ..., e^{j2\pi f(M-1)T_{M-1}}\}, \tag{9}$$

is a diagonal matrix with the Doppler frequency shift, and $\boldsymbol{a}_{Rx}(\theta)$, $\boldsymbol{a}_{Tx}(\theta)$ are the receive and transmit array responses to angle θ, respectively. The ambiguity function, $\tilde{J}(\theta, f, r, \theta_0, f_0, r_0)$, has a main lobe when the hypotheses θ, f, r are close to the target parameters θ_0, f_0, r_0, and has side-lobes for other values of θ, f, r.

As mentioned in Section II, we approximate the detection performance over the entire detection interval by considering the detection at the frame edges of the worst case scenario depicted in Fig. 1. At the frame edges the range difference between the targets is given in (4). By substituting (4) into (6), and then the result into (5), we obtain that the ambiguity function at the edge of the detection interval of Fig. 1 is given by

$$J(\theta, f, \theta_0, f_0) = \Big|\gamma(\theta, f, \theta_0, f_0)\Big|^2 \Big|s\left(\lambda(f_0 - f)T_D/4\right)\Big|^2. \tag{10}$$

Making use of the cyclic shift invariant property of the Trace operator, and that $\boldsymbol{D}(f_0)\boldsymbol{D}(-f) = \boldsymbol{D}(f_0 - f)$, we can express

$$\begin{aligned} \Big|\gamma(\theta, f, \theta_0, f_0)\Big|^2 &= \mathrm{Tr}\Big\{\boldsymbol{Y}^H(\theta, f)\boldsymbol{Y}(\theta_0, f_0)\Big\} = \\ \mathrm{Tr}\Big\{&\boldsymbol{D}(-f)\boldsymbol{C}^H\boldsymbol{a}^*_{Tx}(\theta)\boldsymbol{a}^H_{Rx}(\theta)\boldsymbol{a}_{Rx}(\theta_0)\boldsymbol{a}^T_{Tx}(\theta_0)\boldsymbol{C}\boldsymbol{D}(f_0)\Big\} = \\ &\boldsymbol{a}^H_{Rx}(\theta)\boldsymbol{a}_{Rx}(\theta_0)\boldsymbol{a}^T_{Tx}(\theta_0)\boldsymbol{C}\boldsymbol{D}(f_0 - f)\boldsymbol{C}^H\boldsymbol{a}^*_{Tx}(\theta), \end{aligned} \tag{11}$$

Then, by substituting (11) into (10) we obtain that

$$J(\theta, f, \theta_0, f_0) = g(\theta, \theta_0, \tilde{f}, \boldsymbol{C})\omega(\theta, \theta_0, \tilde{f}), \tag{12}$$

where

$$g(\theta, \theta_0, \tilde{f}, \boldsymbol{C}) = \Big|\boldsymbol{a}^T_{Tx}(\theta_0)\boldsymbol{C}\boldsymbol{D}(-\tilde{f})\boldsymbol{C}^H\boldsymbol{a}^*_{Tx}(\theta)\Big|^2 = \left|\sum_{m=0}^{M-1}\tilde{\boldsymbol{r}}_m e^{-j2\pi\tilde{f}T_m}\right|^2, \tag{13}$$

$$\omega(\theta, \theta_0, \tilde{f}) = \Big|\boldsymbol{a}^H_{Rx}(\theta)\boldsymbol{a}_{Rx}(\theta_0)\Big|^2 \Big|s(-\lambda\tilde{f}T_D/4)\Big|^2, \tag{14}$$

$\tilde{f} = f - f_0$, $\tilde{\boldsymbol{r}}_m$ is the m^{th} element of vector $\tilde{\boldsymbol{r}}$ that is given by

$$\tilde{\boldsymbol{r}} = \boldsymbol{a}^H_{Tx}(\theta)\boldsymbol{C}. * \boldsymbol{a}^T_{Tx}(\theta_0)\boldsymbol{C}, \tag{15}$$

and $.*$ denotes an element wise product (dot-product) operation.

In the case of multiple targets, the match filter output is a superposition of the ambiguity function centered around each target parameters, hence the ambiguity function side-lobes of one target are interfering the detection of another target. The detection performance is mainly dominated by the level of the maximal side-lobe of the ambiguity function. Therefore, high detection performance is achieved when the signal to side-lobe interference ratio (SIR) is maximized with respect to the code, $\boldsymbol{C}$, and the chirps transmission times $\boldsymbol{T}_0, .., T_{M-1}$, where

$$SIR = \frac{J(\theta = \theta_0, f = f_0, \theta_0, f_0)}{\max_{\theta, f \in \Omega} J(\theta, f, \theta_0, f_0)}, \tag{16}$$

and Ω is the Doppler frequencies and angles of the ambiguity function side-lobes.

In order to obtain the same SIR for all target angles, θ_0, the code needs to attain the same ambiguity function main-lobe energy for all target angles. The only set of codes that meets the isometric main-lobe energy constraint, is the set of orthogonal codes [17]. Orthogonal codes have the property that

$$\boldsymbol{C}\boldsymbol{C}^H = \boldsymbol{I}_{N_{Tx}}, \tag{17}$$

where $\boldsymbol{I}_{N_{Tx}}$ is the identity matrix with dimension $N_{Tx} \times N_{Tx}$.

Maximizing the SIR in (16) with respect to a code, $\boldsymbol{C}$, that satisfies (17), and the chirps timings $T_0, .., T_{M-1}$, is a non-convex optimization problem. We have applied numerical optimization techniques for solving this problem, however, they have yield poor performance. Therefore, our solution approach is to design a code and chirp timing pattern that achieves relatively high SIR, based on insights from the ambiguity function expressions (12)-(15). Although this approach does not necessarily achieve the maximal SIR, the results presented in Section IV, show that it achieves superior detection performance over reference methods.

It can be realized from (12), that the ambiguity function is a multiplication of two non-negative terms. The first term, $g(\theta, \theta_0, \tilde{f}, \boldsymbol{C})$, depends on the code and the chirps transmission times, and is equal to the Fourier transform of vector $\tilde{\boldsymbol{r}}$ at frequency $\tilde{f}$. The second term, $\omega(\theta, \theta_0, \tilde{f})$, is independent of the code and chirp timing, and is a function of the range match filtering (range DFT output), $s(-\lambda\tilde{f}T_D/4)$, which is a Sinc function that decays with the increase in the frequency, $\tilde{f}$. Due to Parseval theorem, the total energy of Fourier transform of $\tilde{\boldsymbol{r}}$ is constant. Hence, the side-lobes in $J(\theta, f, \theta_0, f_0)$ will be minimized when $g(\theta, \theta_0, \tilde{f}, \boldsymbol{C})$ is inversely proportional to the function, $\omega(\theta, \theta_0, \tilde{f})$. Since $\omega(\theta, \theta_0, \tilde{f})$ decays with the frequency, $\tilde{f}$, high SIR is attained when the Fourier spectrum of $\tilde{\boldsymbol{r}}$ has smaller energy at lower frequencies than at higher frequencies.

Intuitively, this can be explained as follows. Doppler frequencies that are close to the ambiguity function main-lobe correspond to cases that migration in range difference of interfering targets is small and targets are overlapping in range during the entire detection interval. For higher Doppler frequencies with larger migration, targets are separated in range at some point in the detection interval. Hence, attenuating the side-lobes at frequencies closer to the main-lobe is more important than at frequencies far from the main-lobe.

Based on the insight above, we propose a code that is constructed from repetitions of a short primal orthogonal code with length N_{Tx}, and has linearly increasing chirp transmission time spacing. Next, we will show that this design choice yield a Fourier spectrum of $\tilde{\boldsymbol{r}}$ with desired small energy at low frequencies and larger energy at higher frequencies, and as a results achieves high SIR and good detection performance.

Let $\tilde{\boldsymbol{C}}$ be a short orthogonal code matrix (referred to as primal code) with dimension $N_{Tx} \times Q$, where $Q \geq N_{Tx}$. The proposed code has M/Q repetitions of code $\tilde{\boldsymbol{C}}$, which can be expressed by

$$\boldsymbol{C} = \left[\begin{array}{cccc} \tilde{\boldsymbol{C}} & \tilde{\boldsymbol{C}} & ... & \tilde{\boldsymbol{C}} \end{array}\right]. \tag{18}$$

Since $\tilde{\boldsymbol{C}}$ is orthogonal, then the code in (18) is also orthogonal. For any code of type (18), the vector $\tilde{\boldsymbol{r}}$ is composed M/Q repetitions of the sequence of Q elements $\tilde{r}_0, \tilde{r}_1, .., \tilde{r}_{Q-1}$. The Fourier transform of the vector $\tilde{\boldsymbol{r}}$ in this case has high energy peaks in the frequencies that are integer multiplications of the inverse of the short primal code duration (duration of Q symbols). Therefore, as the primal short code length reduces, the energy of $\tilde{\boldsymbol{r}}$ is concentrated at higher frequencies in the Fourier spectrum, as desired. The shortest orthogonal code length is when $Q = N_{Tx}$, and in this case, when the chirps transmission times are uniformly spaced by δ, the vector $\tilde{\boldsymbol{r}}$ will have energy concentrated at frequencies $k/(N_{Tx}\delta)$, where k is an integer.

Fig. 2 shows an example of the ambiguity function, $J(\theta = \theta_0, f, \theta_0 = 0, f_0 = 0)$, as a function of f, for the case of four transmit antennas, and a code that is composed of 32 repetitions of a Hadamard code of length four. The transmission time difference between chirp symbols (i.e. the symbol duration time) was, $\delta = 100^{-6}s$. The figure also shows the functions $g(\theta, \theta_0, \tilde{f}, \boldsymbol{C})$ and $\omega(\theta, \theta_0, \tilde{f})$ for this case. It is observed, that the function $g(\theta, \theta_0, \tilde{f}, \boldsymbol{C})$ has side-lobes at frequencies replicas of $1/(4 * 100^{-6}) = 2500Hz$, and that these side-lobes are attenuated by the function $\omega(\theta, \theta_0, \tilde{f})$. Therefore, the side-lobes of $J(\theta, \theta_0, \tilde{f})$ are relatively low. Nevertheless, there are still remaining ambiguity function side-lobes peaks at frequencies $k \times 2500$, where k is an integer.

In order to further reduce the ambiguity function side-lobes at frequencies $k/(N_{Tx}\delta)$, we proposed to linearly increase the time difference between transmitted chirps, such that the m^{th} chirp transmission time is given by

$$T_m = T_{m-1} + \delta + m\Delta = m\delta + \sum_{n=0}^{m} n\Delta, \tag{19}$$

where $T_0 = 0$, and Δ is the incremental time step between chirps. As the chirps spacing increases linearly, the side-lobe peaks at frequencies $k/(N_{Tx}\delta)$ are attenuated and their energy is spread over the Doppler frequency band $1/(N_{Tx}\delta)$: $1/(N_{Tx}(\delta + M\Delta))$, where δ is the minimal spacing between chirps (at the beginning of the code sequence), and $\delta + M\Delta$ is the maximal spacing between chirps (at the end of the code sequence).

Fig. 3 shows the term $g(\theta, \theta_0, \tilde{f}, \boldsymbol{C})$ of the ambiguity function for the same code as in Fig. 2, with uniform spacing of $\delta = 100\mu s$ and with two different linearly increasing chirp spacing values of Δ. It is observed that the side-lobes peaks in function $g(\theta, \theta_0, \tilde{f}, \boldsymbol{C})$ are reduced and spread over a wider frequency band as Δ increases.

Determining Δ is a trade-off between two factors that contribute to the SIR. On the one hand, increasing Δ attenuates the energy peaks of $g(\theta, \theta_0, \tilde{f}, \boldsymbol{C})$, which in turn, reduces the ambiguity function side-lobes and thus reduces the SIR. However, on the other hand, as Δ increases the energy of $g(\theta, \theta_0, \tilde{f}, \boldsymbol{C})$ at $k/(N_{Tx}\delta)$ is spread into lower frequencies, in which the value of $\omega(\theta, \theta_0, \tilde{f})$ is high, and as a result, the SIR may be increases. We optimize Δ, by applying a grid search to find the value of Δ that maximizes the SIR expression in (16) given a code (18) with a primal orthogonal code $\tilde{\boldsymbol{C}}$. The optimization neglects the signal to noise ratio reduction as a function of Δ because the SIR is more dominant.

IV. Results and Discussion

We demonstrate the performance of the proposed code and chirp timing design method presented in Section III for the following automotive radar parameters: carrier frequency 77GHz, bandwidth of 1GHz, chirp time $T_u = 100\mu s$, detection interval $T_d = 75msec$, a code sequence length of $M = 128$, and a

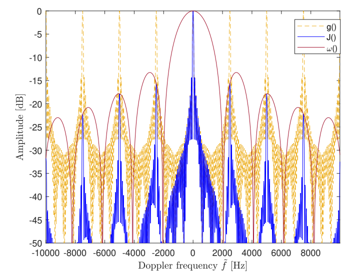

Fig. 2: Ambiguity function, $J()$, and the terms $g()$ and $\omega()$ as a function of $\tilde{f}$ for $\theta_0 = \theta$. The code was 32 repetitions of Hadamard code with 4 symbols.

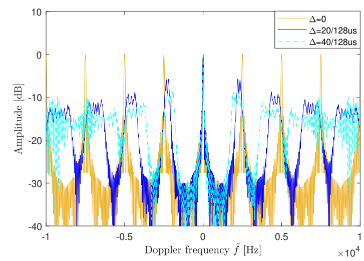

Fig. 3: The term $g(\theta, \theta_0, \tilde{f}, \boldsymbol{C})$ in the ambiguity function as a function of $\tilde{f}$ for repetitive Hadamard code and different chirp spacing increments.

MIMO array with 4 transmit antennas and 4 receive antenna that span a virtual aperture of 16 elements spaced by half a wavelength.

The proposed code was designed according to Section III. The code had 32 repetitions of a primal short Hadamard code with length four. The initial chirps transmission time difference was $\delta = 100\mu s$, and the spacing increased linearly by $\Delta = 0.1563\mu s$, which maximized the SIR in (16). We also tested three reference methods. The first reference method, had the same code sequence as the proposed method but with uniform chirp spacing of $100\mu s$, i.e. $\Delta = 0$. The second reference method, is a long Hadamard code with length 128 symbols, and uniform chirp spacing of $100\mu s$ ($\Delta = 0$). The third reference method, had the same code sequence as the second method, but with linearly increasing chirp spacing of $\Delta = 0.117\mu s$, which maximized the SIR in (16).

Fig. 4, shows the ambiguity function along the Doppler domain at $\theta = \theta_0$, for the proposed method and all three reference methods. It is observed from the figure that the proposed repetitive short Hadamard code with linear increasing chirp transmission time spacing (blue curve) attains lower side-lobes than all reference method. Furthermore, linear increasing chirps spacing has negligible side-lobes reduction for long orthogonal code. It is the combination of repetitive short orthogonal code and linearly increasing chirps spacing that reduces the ambiguity function side-lobes significantly.

Fig. 5 shows the receiver operating characteristic (ROC) performance of the proposed code and the three reference codes, for the same parameters that were tested in Figs. 4.

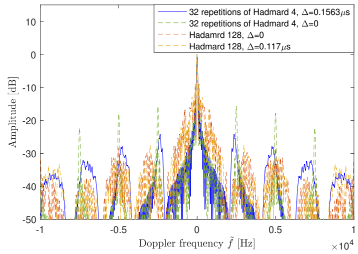

Fig. 4: Ambiguity function 1D slice in the Doppler domain for all tested methods.

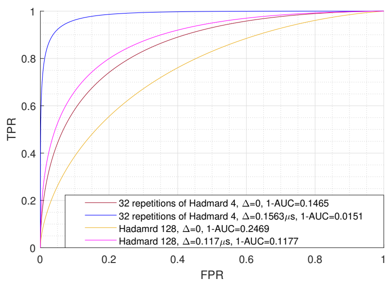

Fig. 5: ROC performance comparison between tested methods.

For the ROC simulation we tested two targets that were at the same range in the middle of the detection interval. One target was considered as a desired target, and the other target was an interfering target that had 13 dB higher energy than the desired target. The signal to noise ratio of the desired target was 15 dB when $\Delta = 0$, and it reduced according to signal duty cycle reduction when $\Delta > 0$ (accounting for the power reduction). The desired target was at $\theta_0 = 0, f_0 = 0$, and the angle and Doppler frequency of the interfering target was randomly selected in each realization outside of the desired target main-lobe region, thus its side-lobe were interfering the desired target. The output of the match filter receiver (after range DFT, Doppler DFT and beamforming) was compared to a detection threshold. Per each detection threshold value in the ROC calculation, a positive detection was counted when the energy in the desired target angle and Doppler ($\theta_0 = 0, f_0 = 0$) was above the threshold. A false detection was counted when the match filter output energy at some angle and Doppler outside of the desired and interfering targets ambiguity function main-lobe regions was above the threshold.

The results in Fig. 5 shows that the proposed coding method achieves a significant performance advantage in term of probability of detection compared to the other reference methods. The area above the ROC curve of the proposed code (one minus the ROC area under the curve (AUC)), is an order of magnitude lower than the best reference method. This area is the probability that a randomly selected measurement with only noise and interference (without the desired target signal) will have higher energy than a randomly selected measurement of the desired signal with interference and noise. When this event occurs the radar cannot distinguish between the desired signal and the interference plus noise for any threshold.

V. Conclusions

This paper introduces a method for designing a code and chirp transmission times for FMCW CDMA MIMO automotive radar that attains high detection performance in the case of multiple targets that overlap in range during a detection interval. We derived an analytical expression for the ambiguity function of the radar that takes into account migration in the range difference of the interfering targets during the detection interval. The analytical expression provides insight that the code and chirp transmission times need to attenuate the ambiguity function side-lobes at Doppler frequencies that are close to the main-lobe. We propose a code sequence that meets this objective. The code is composed of repetitions of short orthogonal code with linearly increments of the time difference between chirps. The proposed code showed lower ambiguity function side-lobes and significantly better detection performance compared to reference codes.

References

[1] J. Dickmann, J. Klappstein, M. Hahn, N. Appenrodt, H. Bloecher, K. Werber, A. Sailer, "Automotive radar the key technology for autonomous driving: From detection and ranging to environmental understanding", *IEEE Radar Conference*, 2016.

[2] I. Bilik, O. Bialer, S. Villeval, H. Sharifi, K. Kona, M. Pan, D. Persechini, M. Musni, K. Geary, "Automotive MIMO Radar For Urban Environments", *IEEE Radar Conference*, 2016.

[3] H. Sun, F. Brigui, M. Lesturgie, "Analysis and Comparison of MIMO Radar Waveforms," *International Radar Conference*, Oct. 2014.

[4] Z. Tong, R. Renter and M. Fujimoto, "Fast chirp FMCW radar in automotive applications," *IET International Radar Conference*, 2015.

[5] W. van Rossum and L. Anitori, "Doppler ambiguity resolution using random slow-time code division multiple access MIMO radar with sparse signal processing," *IEEE Radar Conference*, 2018.

[6] M. Mbeutcha and V. Krozer, "CDMA-based MIMO FMCW Radar System Performance using Intra-Pulse Phase Modulation," *16th European Radar Conference (EuRAD)*, 2019.

[7] G. San Antonio, D. R. Fuhrmann, and F. C. Robey, "MIMO radar ambiguity functions," *IEEE J. Sel. Topics in Signal Process.*, vol. 1, pp. 167–177, Jun. 2007.

[8] J.Wolfmann, "Almost perfect autocorrelation sequences," *IEEE Trans. on Information Theory*, vol. 38, no. 4, pp. 1412–1418, Jul. 1992.

[9] X. H. Tang, P. Z. Fan, and S. Matsufuji, "Lower bounds on correlation of spreading sequence set with low or zero correlation zone," *Electron. Lett.*, vol. 36, no. 6, pp. 551–552, Mar. 2000.

[10] A. Tang, R. Carey, G. Virbila, Y. Zhang, R. Huang and M. Frank Chang, "A Delay-Correlating Direct-Sequence Spread-Spectrum (DS/SS) Radar System-on-Chip Operating at 183–205 GHz in 28 nm CMOS," *IEEE Trans. on Terahertz Science and Technology*, vol. 10, no. 2, pp. 212-220, March 2020.

[11] C. Chen and P. P. Vaidyanathan, "MIMO Radar Waveform Optimization With Prior Information of the Extended Target and Clutter," *IEEE Trans. on Signal Processing*, vol. 57, no. 9, pp. 3533-3544, Sept. 2009.

[12] K. Iwasa, T. Kishigami, H. Yomo, A. Matsuoka and J. Satou, "MIMO radar system using orthogonal complementary codes with Doppler offset," *European Radar Conference (EURAD)*, 2017.

[13] I. Pasya and T. Kobayashi, "Simulation of time jitter effects on the detection performance of M-sequence-based MIMO radar systems," *IEEE Radio and Wireless Symposium*, 2013.

[14] J. Overdevest, F. Jansen, F. Uysal and A. Yarovoy, "Doppler Influence on Waveform Orthogonality in 79 GHz MIMO Phase-Coded Automotive Radar," *IEEE Trans. on Vehicular Technology*, vol. 69, no. 1, pp. 16-25, Jan. 2020.

[15] J. Tang, N. Zhang, Z. Ma and B. Tang, "Construction of Doppler Resilient Complete Complementary Code in MIMO Radar," *IEEE Trans. on Signal Processing*, vol. 62, no. 18, pp. 4704-4712, Sept.15, 2014.

[16] H. Rohling, "Radar CFAR Thresholding in Clutter and Multiple Target Situations," *IEEE Trans. on Aerospace and Elect. Systems*, Vol. AES-19, Issue 4, pp. 608-621, July 1983.

[17] R. A. Horn, C. R. Johnson, Matrix Anlysis, Cambridge University Press. 2013.